Acta Crystallographica Section F
Structural Biology and Crystallization Communications
ISSN 1744-3091

Crystallization and X-ray diffraction analysis of the Trp/amber editing site of hepatitis delta virus (+)RNA: a case of rational design

Celeste MacElrevey and Joseph E. Wedekind*

Department of Biochemistry and Biophysics, University of Rochester School of Medicine and Dentistry, Rochester, New York 14642, USA

Correspondence e-mail: joseph_wedekind@urmc.rochester.edu

Received 16 September 2005
Accepted 2 November 2005
Online 12 November 2005

RNA editing by mammalian ADAR1 (Adenosine Deaminase Acting on RNA) is required for the life cycle of the hepatitis delta virus (HDV). Editing extends the single viral open reading frame to yield two protein products of alternate length. ADARs are believed to recognize double-stranded RNA substrates *via* a 'structure-based' readout mechanism. Crystals of 10-mer duplexes representing the HDV RNA-editing site diffracted to 1.35 Å resolution, but suffered from merohedral twinning and averaging of the base registry. Expansion of the construct to include two flanking 3 × 1 internal loops yielded crystals in the primitive tetragonal space group $P4_12_12$ or $P4_32_12$. X-ray diffraction data were collected to 2.8 Å resolution, revealing a unit cell with parameters a = 62.5, c = 63.5 Å. The crystallization and X-ray analysis of multiple forms of the HDV RNA-editing substrate, encounters with common RNA crystal-growth defects and a strategy to overcome these problems are reported.

1. Introduction

RNA editing by members of the ADAR family converts adenosine to inosine through hydrolytic base deamination of the C6 exocyclic amine (Polson *et al.*, 1991). This activity fulfills two roles. Site-specific nuclear editing of endogenous mRNA transcripts diversifies the proteome (Bass, 2002), while promiscuous editing of duplex RNA has implications in RNAi and viral defense (George & Samuel, 1999; Tonkin & Bass, 2003). The key to these dual functions resides to some extent in the RNA structure itself. Duplex mismatches contribute to bulging of targeted adenosines (Yi-Brunozzi *et al.*, 2001), although base-paired substrates also exist. Internal loops may act to either prevent binding of ADARs, thereby directing the enzyme to neighboring base-paired regions, or to create recognition sites through localized bending or widening of RNA grooves (Lehmann & Bass, 1999).

ADAR1 edits within the only open reading frame of the hepatitis delta virus, a subviral pathogen associated with chronic hepatitis B infection (Rizzetto, 1983; Polson *et al.*, 1996). ADAR1 targets A1012 of an A·C mismatch within a double-stranded region of the ∼1700-nucleotide circular single-stranded HDV RNA anti-genome. Although there are multiple A·C mismatches in the HDV genome, editing is exclusive to A1012. The UAG amber 'stop' codon is edited to UIG, which is decoded by the ribosome as the tryptophan codon UGG. This modified transcript generates a new delta antigen protein (HDAg-p27) that is 19 amino acids longer than the unedited precursor (HDAg-p24). These two forms are reciprocally required in the viral life cycle; p24 enhances transcription, whereas p27 allows packaging (Kuo *et al.*, 1989; Ryu *et al.*, 1992).

To provide insight into the special structural features of RNA that promote ADAR1 binding and editing, we undertook a structural analysis of several minimal substrates. This manuscript describes our progress towards a structure of the HDV editing site. Specifically, we document encounters with crystal twinning and base-averaging, as well as strategies to overcome this problem that should be applicable to the crystallization of RNA helices.

Table 1
X-ray diffraction data and refinement statistics.

Values in parentheses are for the highest resolution shell.

	Edited 10 × 10	Unedited 10 × 10	Edited 23 × 19
Data collection			
Space group	*H*3	*H*3	$P4_12_12$ or $P4_32_12$
Unit-cell parameters (Å)	*a* = 39.5, *c* = 246.4	*a* = 49.0, *c* = 235.8	*a* = 62.5, *c* = 63.6
Resolution	29.92–1.35 (1.40–1.35)	23.38–2.85 (2.95–2.85)	36.29–2.80 (2.90–2.80)
Total reflections	122008	16052	16572
Unique reflections	30558	4798	3307
Redundancy	3.99 (1.78)	3.35 (3.67)	5.01 (4.82)
Completeness (%)	96.8 (77.4)	97.2 (99.8)	97.0 (92.7)
$\langle I/\sigma(I)\rangle$	13.1 (2.2)	10.3 (1.9)	11.4 (2.2)
R_{sym}† (%)	6.3 (35.4)	6.1 (37.9)	9.9 (33.4)
Twinning fraction	0.38	0.41	None
Refinement statistics			
Resolution	30.0–1.5		
No. of atoms (RNA/water)	1257/26		
R_{work}‡/R_{free}§ (%)	31.9/31.8		
R.m.s.d. bonds (Å)	0.0038		
R.m.s.d. angles (°)	0.94		

† $R_{sym} = \sum|I_j - \langle I_j\rangle|/\sum|I_j| \times 100$. ‡ $R_{work} = \sum_{hkl}|F_o - kF_c|/\sum_{hkl}|F_o| \times 100$. R_{work} was calculated using 93% of the data. § R_{free} is defined as the R_{work} calculated using 7% of the data selected randomly and excluded from the refinement.

2. Materials and methods

2.1. Materials

RNA oligonucleotides were synthesized by Dharmacon Inc. (Lafayette, CO, USA). Polyethylene glycol monomethyl ether (PEG MME) and triethylamine (TEA) were from Fluka (Buchs, Switzerland). Spermidine was from Sigma (Milwaukee, WI, USA). HPLC-grade acetonitrile was from JT Baker (Phillipsburg, NJ, USA) and glycerol was from MP Biomedicals (Irvine, CA, USA). All other chemicals were from Fisher Scientific (Fairlawn, NJ, USA). Crystal Tools were from Nextal (Montreal, QC, Canada); VDX plates and silanized glass cover slips were from Hampton Research (Laguna Niguel, CA, USA). Cover slips were autoclaved prior to use. All water was autoclaved and originated from a UV/UF Nanopure Infinity water-polishing system (Barnstead, IA, USA).

2.2. RNA purification

Oligonucleotides were deprotected according to the manufacturer's instructions, except that heating was for 1 h at 338 K. Individual RNA strands were purified on a 1.9 × 30 cm μBondapack C18 column (Waters, Milford, MA, USA) on a Waters HPLC equipped with Model 510 pumps, an automated gradient controller and a Waters 484 MS Absorbance Detector interfaced with the *MacIntegrator* software (Varian, Palo Alto, CA, USA). HPLC separations employed the TEA/TEAA (triethyl ammonium acetate) ion-pairing system at pH 7.0. Buffer *A* was 0.1 *M* TEA/TEAA; buffer *B* comprised buffer *A* plus 50%(*v*/*v*) acetonitrile. Preparative-scale RNA separations were eluted at 7 ml min^{-1} with linear gradients using 15–30%(*v*/*v*) buffer *B* over 60 min intervals. RNA elution was monitored at 260 nm; fractions were pooled and lyophilized to ∼1 ml volume. Concentrated RNA was desalted using SepPak Vac C18 cartridges (Waters), which entailed loading, water washing and batch elution with 40%(*v*/*v*) acetonitrile. Variations of HPLC purification and desalting have been described previously (Wedekind & McKay, 2000). Individual strands of desalted RNA were lyophilized to dryness and resuspended in 10 m*M* sodium cacodylate buffer pH 6.0 to a final working concentration of 1–2 m*M*. Equimolar concentrations were mixed to a final concentration of 0.5 m*M* for the 10 × 10-mer and 0.9 m*M* for all other constructs. Annealing was performed on longer constructs at 348 K for 5 min, followed by slow-cooling to room temperature. Samples were spun for 10 min at 12 045*g* at 277 K prior to crystal setups.

2.3. Crystallization

Eight unique HDV RNA constructs were subjected to crystallization by hanging-drop vapor diffusion at 293 K based on screens previously established for small ribozymes (Wedekind & McKay, 2000; Grum-Tokars *et al.*, 2003). *RNAstructure* v.4.2 was used as a design resource for thermodynamic folding calculations (Mathews *et al.*, 2004) (Fig. 1). A volume of 1 µl precipitating agent from a 1 ml reservoir was added to 1 µl RNA. Precipitants included combinations of Li^+, Na^+, K^+, NH_4^+ or Mg^{2+} with counterions Cl^-, SO_4^{2-} or acetate, as well as high-molecular-weight polymers PEG and PEG MME. All trials included 2 m*M* spermidine, 10 m*M* $MgCl_2$ and 0.1 *M* sodium cacodylate buffer pH 6.0. Droplets were examined 3–6 d after setup and weekly thereafter by use of an 80× MZ9.5 dissecting microscope (Leica, Wetzler, Germany) equipped with a polarizer and analyzer.

2.3.1. Streak-seeding, microseeding and macroseeding. To improve crystal quality and size, three seeding methods were employed in conjunction with other optimization methods. Streak-seeding was performed on equilibrated drops containing 1:1 mixtures of RNA and reservoir solution. A natural fiber was dragged once through an over-nucleated 'source' drop, then once through a clear 'receiving' drop at lower precipitant concentration. For microseeding, over-nucleated crystals were crushed, serially diluted (10- to 10^6-fold) with mother liquor and 0.5 µl was added to the receiving drop. For macroseeding, small crystals were transferred using either a 20 µm rayon loop (Hampton Research) or a P10 Gilson pipette (Middleton, WI, USA) into a receiving drop with 0–5% less precipitant. Receiving drops were prepared 24 h prior to seeding with 2 µl each of precipitant and RNA at concentrations of 0.5 or 0.9 m*M*.

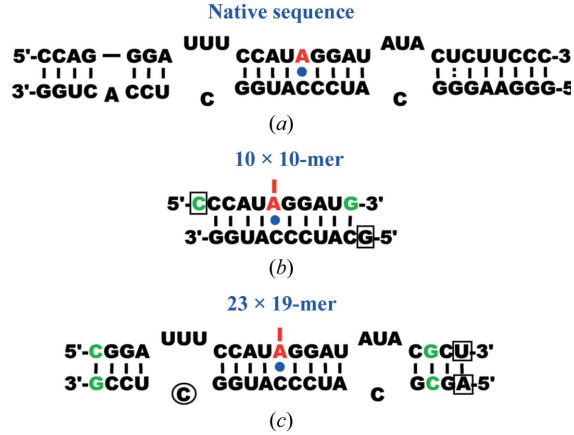

Figure 1
Schematic diagram of HDV RNA secondary structures harboring the Trp/amber editing site at an A·C mismatch (inosine shown above). Mutations from the native sequence are in green. Boxed or circled bases were removed during construct development to optimize crystallization. (*a*) A double-stranded region of the native antigenomic RNA. The edited position is shown in red. (*b*) The 10 × 10-mer minimal substrate constructs, including sticky-ended and blunt-ended, edited and unedited versions (four in total). (*c*) The asymmetric 23 × 19-mer crystallization constructs (edited and unedited). The 23 × 19-mer was truncated to an edited 22 × 18-mer and then to a 22 × 17-mer, both of which were used in crystallization trials without success.

2.4. X-ray diffraction experiments

Single crystals were cryoprotected by 3 min serial transfers through synthetic mother liquors containing 5, 10, 15 and 20%(*v*/*v*) glycerol or MPD. Crystals were captured by surface tension in 20 µm rayon loops and flash-cooled to 100 K in a stream of cold nitrogen gas generated by an X-stream (Rigaku/MSC, TX, USA). X-rays were generated by an RU-H2R rotating-anode generator (Rigaku/MSC) operated at 4.5 kW and equipped with a 0.3 mm focal cup. X-rays were filtered and focused by confocal optics (Rigaku/MSC) and collimated through a 0.5 mm front-end pinhole. Diffraction data were recorded on an R-AXIS IV image-plate detector equipped with a vertical φ-rotation axis at a crystal-to-detector distance of 15 cm. A total of 78° was collected for the 23 × 19-mer as 0.5° oscillations per 15 min exposure.

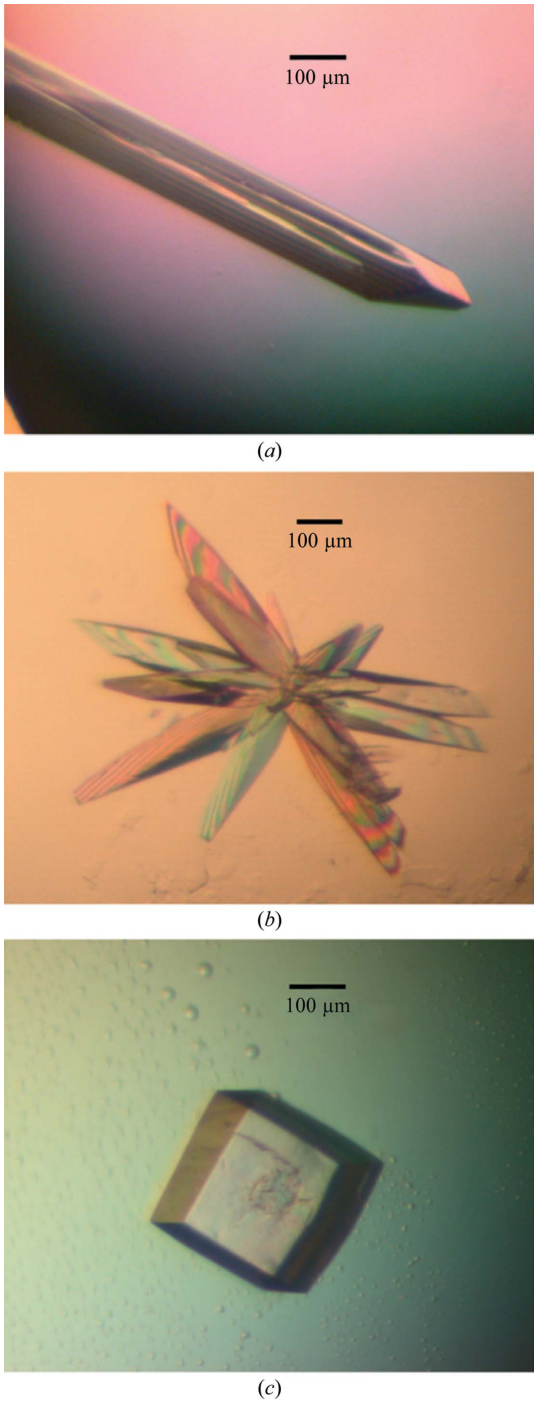

Figure 2
Representative crystals of the HDV Trp/amber RNA-editing site. (*a*) Unedited 10 × 10-mer RNA constructs grew as 1 mm rods with a diameter of 0.1 mm. (*b*) Edited 10 × 10-mer crystals displaying a trigonal habit are 0.5 mm in length (*c*). Edited 23 × 19-mer crystals grown from macroseeding experiments reached 0.25 mm in each dimension. Crystals were photographed under polarized light.

Additional data were collected at station A1 of the Cornell High Energy Synchrotron Source (CHESS, Ithaca, NY, USA) using a Quantum 210 CCD detector (ADSC, Poway, CA, USA) at crystal-to-detector distances of 13.5 and 15.0 cm for the edited and unedited 10 × 10 samples, respectively. Data were collected with a $\Delta\varphi$ of 0.5° per image and exposure times of 20–30 s, totaling 140 and 120°, respectively. An additional low-resolution pass was collected for the edited crystal at a distance of 30 cm with an exposure time of 3 s per 0.5°. Intensities were reduced and merged with *CrystalClear* (Pflugrath, 1999). X-ray diffraction and data-reduction statistics are reported in Table 1.

2.5. Structure determination, refinement and twinning analysis

Structures of the RNA duplexes were solved by molecular replacement using *AMoRe* (Navaza, 2001). Amplitudes were generated by *TRUNCATE*, a component of *CCP*4 (Collaborative Computational Project, Number 4, 1994). Structures were refined in *CNS* (Brünger *et al.*, 1998) and electron-density maps were examined in *O* (Jones *et al.*, 1991). Twinning was diagnosed on the Merohedral Crystal Twinning Server (http://nihserver.mbi.ucla.edu/Twinning/) courtesy of the Todd Yeates laboratory using 95.5% of reflections from 3 to 6 Å resolution (Yeates, 1997). Detwinning was performed in *CNS*. Refinement statistics for the edited 10 × 10-mer are reported in Table 1.

3. Results and discussion

3.1. 10 × 10-mer results

3.1.1. Crystallization screening. The initial target of these studies focused on duplex 10-mers encompassing the minimal substrate capable of supporting ADAR1 activity (Sato *et al.*, 2001). A·C mismatch and I·C base-pair targets were tested in both blunt-ended and sticky-ended configurations (Fig. 1*b*). Crystals grew quickly for all four constructs, producing showers of needles in 0.5 *M* lithium, sodium and potassium acetate with 15–30%(*w*/*v*) PEG 2000 MME; additional crystals were observed in 0.5–3.8 *M* solutions of lithium, magnesium and ammonium sulfate with and without PEG 2000 MME. Streak-seeding was performed on clear drops, yielding single crystals in the form of long rods of ∼1.0 × 0.1 × 0.1 mm in size for the blunt-ended unedited construct and in a trigonal habit of dimensions 0.5 × 0.15 × 0.15 mm for the blunt-ended edited crystals (Figs. 2*a* and 2*b*).

3.1.2. Diffraction experiments. Edited crystals (Fig. 2*b*) were serially cryoprotected in a synthetic mother liquor containing 20%(*v*/*v*) glycerol, 30%(*w*/*v*) PEG 2000 MME, 0.10 *M* sodium cacodylate, 2 m*M* spermidine, 10 m*M* magnesium chloride and 0.50 *M* lithium acetate. Crystals diffracted to 1.6 Å resolution in-house and to better than 1.4 Å resolution using synchrotron radiation (Table 1). The space group and unit-cell parameters were determined to be rhombohedral and were treated in the hexagonal setting *H*3, with a = 39.4, c = 248.2 Å. Low- and high-resolution synchrotron-derived data sets were integrated together during processing with *CrystalClear*. An analysis of the Matthews coefficient by *CCP*4 suggested two or three 10-mer duplexes (20 or 30 nucleotides) per

asymmetric unit (V_M = 2.9 Å^3 Da^{-1} with 58% solvent content or V_M = 2.0 Å^3 Da^{-1} with 36.6% solvent content).

Unedited crystals (Fig. 2*a*) were cryoprotected similarly with a synthetic mother liquor containing 20%(*v*/*v*) glycerol, 0.10 m*M* sodium cacodylate, 2 m*M* spermidine, 10 m*M* magnesium chloride and 2.3 *M* ammonium sulfate. These crystals diffracted anisotropically to ∼3 Å resolution at home. The crystals indexed as *H*3 with unit-cell parameters *a* = 49.1, *c* = 239.5 Å. The difference between edited and unedited unit cells (10 Å along the *a* and *b* axes and 9 Å along the *c* axis) was considerable, given the single atom change between constructs. Data collection at CHESS extended the resolution of the unedited construct to 2.8 Å (Table 1). An analysis of the V_M gave a value of 2.9 Å^3 Da^{-1} (56.8% solvent content), consistent with three molecules per asymmetric unit.

3.1.3. Structure determination and twinning. The edited crystal was solved by molecular replacement using a 10-mer duplex search model derived from PDB entry 405d (Pan *et al.*, 1998). Trials to independently place one model in three positions using data from 2.0 to 15 Å resolution yielded a correlation coefficient of 80.1% with an *R* factor of 44%. Refinement proceeded in *CNS*, with 7% of the data reserved for cross-validation (R_{free}). After rigid-body refinement, positional and individual *B*-factor refinement, R_{work} failed to drop below 35%. Inspection of electron-density maps prompted submission of diffraction data to the Merohedral Crystal Twinning Server, which identified a positive result for a twofold operator in the [110] plane. Considerable twinning fractions were obtained for all 10-mer duplex data sets, ranging from 0.35 to 0.45. The *CNS* routine 'detwin partials' was implemented with a twinning fraction of 0.38 and refinement repeated (Table 1). Electron-density maps were much improved. Specifically, the electron density for ribose and phosphates was well resolved; however, the base density was incomplete and R_{work} could not be brought below 30% at 1.6 Å resolution. This was likely to be a result of base-averaging owing to the high symmetry of the construct, as previously observed by Shah & Brünger (1999). Analysis of the existing model using *CURVES* suggested that this duplex may exhibit some A′-form character, including a widened major groove and a decreased inclination angle (Lavery & Sklenar, 1988; Stofer & Lavery, 1994). Poly(I)-poly(C) RNA is known to form A′-form RNA; however, this has not been documented to result from a single inosine (Arnott *et al.*, 1973). The fully refined structure will determine whether this deviation is a propagated effect of the single IC pair or possibly a result of localized translational averaging of the duplex.

The unedited construct was also solved by molecular replacement using the edited model of this study, which was divided into two search models, a 20-mer duplex and a 10-mer duplex. Utilizing data between 2.9 and 15 Å yielded a correlation coefficient of 57.4% with an *R* factor of 52.6%. Packing suggested a potential solution, although a 6.9 Å gap existed between end-to-end packing molecules. Detwinning (twin fraction 0.41) and subsequent refinement yielded traceable phosphate backbones in electron-density maps, although these were of much poorer quality owing to the lower resolution and anisotropy of the diffraction data. These data were set aside when R_{work} could not be brought below 49%.

3.2. 23 × 19-mer results

3.2.1. Crystallization. Following the experience of twinning and base-averaging, RNA crystallization constructs were expanded to include two flanking 3 × 1 internal loops within the endogenous HDV sequence (Fig. 1*a*), thereby eliminating the high symmetry of the 10-mers. Two modest modifications were made to the native sequence to promote folding and stability: (i) a closing G–C pair was reversed to C–G and (ii) a stem U·G wobble pair was converted to a G–C pair (Fig. 1*c*). The final blunt-ended construct incorporated a 23-nucleotide edited strand and a complementary 19-mer.

Screening yielded small crystals 7–14 d after setup in conditions consisting of 0.5 *M* sodium, lithium and potassium acetate with ∼25%(*w*/*v*) PEG 2000 MME for both edited and unedited constructs. Additional edited crystals were observed in 2.5 *M* ammonium sulfate. Crystals from acetate salts diffracted to ∼10 Å resolution after cryoprotection in 10%(*v*/*v*) glycerol. Further cryoprotection induced cracking. Increasing the acetate and PEG concentrations yielded edited crystals with a cubic habit and dimensions of ∼150 µm. These crystals diffracted to 5 Å resolution after serial cryoprotection to 20%(*v*/*v*) glycerol. A series of microseeding and macroseeding experiments were performed to increase crystal size. Macroseeding proved successful for I·C crystals and although deformations could be visualized, these crystals diffracted to ∼4 Å resolution when capillary-mounted and exposed on the home X-ray source. Beginning as a 100 µm^3 seed, the best macroseeded crystal grew to 0.25 × 0.2 × 0.2 mm (Fig. 2*c*) after four weeks in conditions consisting of 0.75 *M* potassium acetate and 25%(*w*/*v*) PEG 2000 MME. This crystal form diffracted to 2.8 Å resolution at home after cryoprotection in MPD; MPD was used as a cyroprotectant after trials in PEG 550, sucrose, ethylene glycol and glycerol were observed to damage crystals. Attempts to improve crystal growth by removing the last A–U base pair (making a 22 × 18-mer; Fig. 1*c*) and by converting the first 3 × 1 internal loop into a three-nucleotide bulge loop (22 × 17-mer; Fig. 1*c*) yielded no crystals.

3.2.2. Diffraction experiments. *CrystalClear* indexed the 23 × 19-mer crystals as cubic. However, crystals appeared to be birefringent and reduction in space group *P*23 produced an R_{merge} of 61%; data were therefore processed as *P*422. Analysis of V_M suggested one molecule per asymmetric unit with a value of 2.3 Å^3 Da^{-1} and a solvent content of 47%. Zones displaying systematically absent reflections were measured and $I/\sigma(I)$ values for the *h*00 reflection class were consistent with screw axes along *a* and *b* (2*n* present, where *n* is an integer). Similarly, the 00*l* reflections supported a 4_1 or 4_3 screw axis along the *c* axis (4*n* present). This analysis suggested space group $P4_12_12$ or its enantiomorph. These space groups are not susceptible to twinning. The presence of systematic absences in $P4_12_12$ (or $P4_32_12$) supports the case that these crystals are not twinned.

3.2.3. Structure-determination efforts. Multiple molecular-replacement attempts with *AMoRe* and *Phaser* v.3.1 (McCoy *et al.*, 2005) failed to produce a satisfactory solution using models derived from PDB entries 1sdr, 405d or 1nuj (Schindelin *et al.*, 1995; Pan *et al.*, 1998; Wedekind & McKay, 2003). Experimental MAD phasing methods using halogenated bases, 2′-deoxy-2′-selenoribose or 5′-selenoribose are currently being pursued (Teplova *et al.*, 2002).

This work was funded in part by NIH grant GM63162 (JEW) and T32 training award GM068411 (CM). The authors thank Jolanta Krucinska for assistance with crystal growth and the staff of CHESS for assistance with data collection at the A1 station. CHESS is supported by the NSF under award DMR-0225180 and NIH through NCRR award RR-01646.

References

Arnott, S., Hukins, D. W., Dover, S. D., Fuller, W. & Hodgson, A. R. (1973). *J. Mol. Biol.* **81**, 107–122.
Bass, B. L. (2002). *Annu. Rev. Biochem.* **71**, 817–846.

Brünger, A. T., Adams, P. D., Clore, G. M., DeLano, W. L., Gros, P., Grosse-Kunstleve, R. W., Jiang, J.-S., Kuszewski, J., Nilges, M., Pannu, N. S., Read, R. J., Rice, L. M., Simonson, T. & Warren, G. L. (1998). *Acta Cryst.* D**54**, 905–921.
Collaborative Computational Project, Number 4 (1994). *Acta Cryst.* D**50**, 760–763.
George, C. X. & Samuel, C. E. (1999). *Proc. Natl Acad. Sci. USA*, **96**, 4621–4626.
Grum-Tokars, V., Milovanovic, M. & Wedekind, J. E. (2003). *Acta Cryst.* D**59**, 142–145.
Jones, T. A., Zou, J. Y., Cowan, S. W. & Kjeldgaard, M. (1991). *Acta Cryst.* A**47**, 110–119.
Kuo, M. Y., Chao, M. & Taylor, J. (1989). *J. Virol.* **63**, 1945–1950.
Lavery, R. & Sklenar, H. (1988). *J. Biomol. Struct. Dyn.* **6**, 63–91.
Lehmann, K. A. & Bass, B. L. (1999). *J. Mol. Biol.* **291**, 1–13.
McCoy, A. J., Grosse-Kunstleve, R. W., Storoni, L. C. & Read, R. J. (2005). *Acta Cryst.* D**61**, 458–464.
Mathews, D. H., Disney, M. D., Childs, J. L., Schroeder, S. J., Zuker, M. & Turner, D. H. (2004). *Proc. Natl Acad. Sci. USA*, **101**, 7287–7292.
Navaza, J. (2001). *Acta Cryst.* D**57**, 1367–1372.
Pan, B., Mitra, S. N. & Sundaralingam, M. (1998). *J. Mol. Biol.* **283**, 977–984.
Pflugrath, J. W. (1999). *Acta Cryst.* D**55**, 1718–1725.
Polson, A. G., Bass, B. L. & Casey, J. L. (1996). *Nature (London)*, **380**, 454–456.
Polson, A. G., Crain, P. F., Pomerantz, S. C., McCloskey, J. A. & Bass, B. L. (1991). *Biochemistry*, **30**, 11507–11514.
Rizzetto, M. (1983). *Hepatology*, **3**, 729–737.
Ryu, W. S., Bayer, M. & Taylor, J. (1992). *J. Virol.* **66**, 2310–2315.
Sato, S., Wong, S. K. & Lazinski, D. W. (2001). *J. Virol.* **75**, 8547–8555.
Schindelin, H., Zhang, M., Bald, R., Furste, J. P., Erdmann, V. A. & Heinemann, U. (1995). *J. Mol. Biol.* **249**, 595–603.
Shah, S. A. & Brünger, A. T. (1999). *J. Mol. Biol.* **285**, 1577–1588.
Stofer, E. & Lavery, R. (1994). *Biopolymers*, **34**, 337–346.
Teplova, M., Wilds, C. J., Wawrzak, Z., Tereshko, V., Du, Q., Carrasco, N., Huang, Z. & Egli, M. (2002). *Biochimie*, **84**, 849–858.
Tonkin, L. A. & Bass, B. L. (2003). *Science*, **302**, 1725.
Wedekind, J. E. & McKay, D. B. (2000). *Methods Enzymol.* **317**, 149–168.
Wedekind, J. E. & McKay, D. B. (2003). *Biochemistry*, **42**, 9554–9563.
Yeates, T. O. (1997). *Methods Enzymol.* **276**, 344–358.
Yi-Brunozzi, H. Y., Stephens, O. M. & Beal, P. A. (2001). *J. Biol. Chem.* **276**, 37827–37833.